A Long-Wavelength Hosing Instability in Laser-Plasma Interactions

B. J. Duda, R. G. Hemker, K. C. Tzeng, and W. B. Mori

Departments of Physics and Astronomy and Electrical Engineering, University of California at Los Angeles, Los Angeles, California 90095

(Received 24 December 1998)

The nonlinear final state of short-pulse lasers is examined using fully explicit particle-in-cell simulations. A new long-wavelength hosing instability is found to be dominant after a few Rayleigh lengths of propagation. This instability causes self-trapped electrons to be displaced off axis; we find that ion motion is important at the highest densities studied. A possible explanation for this instability is given based on a new variational principle analysis for short-pulse lasers propagating in underdense plasma.

PACS numbers: 52.40.Nk, 52.35.Py, 52.60.+h, 52.65.Rr

Understanding the evolution of short-pulse high-intensity lasers as they propagate through underdense plasmas is essential for the successful development of some plasma accelerator [1] and radiation schemes [2], as well as for the fast ignitor fusion concept [3]. As a result, there has been much research during the past few years on short-pulse laser-plasma interactions. This work has resulted in the identification of numerous self-modulated processes, e.g., relativistic self-focusing [4], ponderomotive blowout/cavitation, and Raman forward scattering (RFS) instabilities [5,6], including envelope self-modulation [7] and hosing [8,9]. While the work of the past few years has led to the determination of the spatiotemporal growth behavior of the above processes [5–9], it is not clear which, if any, of these processes dominate the evolution of the laser after these processes have saturated.

In this Letter, we use the particle-in-cell (PIC) model PEGASUS [10] to investigate the final nonlinear state of short-pulse lasers after they have propagated through a few Rayleigh lengths of plasma. We find over a wide parameter space that the laser's evolution follows a common sequence of events. Furthermore, we find that the final state of the laser is dominated by a new long-wavelength hosing instability. We present a variational principle analysis which provides the growth rate for the well-known Raman-type hosing instability [8,9], but which clearly identifies a long-wavelength hosing (LWH) regime. At higher densities, we find ion motion to be important. Finally, we illustrate through PIC simulations that a consequence of LWH is for the self-trapped electrons [11] to be displaced sideways.

We begin by presenting results from a PEGASUS simulation in which a 600 fs/μm laser is focused with a peak intensity of 5×10^{18} W/cm^2 and a spot size of 20 μm onto the edge of a 1.4×10^{19} plasma slab. For these parameters, $\omega_0/\omega_p = 8.5$, $c/\omega_p = 1.36$ μm, the Rayleigh length is $x_R = 1.2$ mm, the peak normalized vector potential $a_0 = eA_0/mc^2 = 2$, and the ratio of laser power to the critical power for relativistic self-focusing is [4] $P/P_c = a^2(k_p w)^2/32 = 27$. In the simulation 1.2×10^7 electrons are followed on a 8192×256 x-y Cartesian grid, while the ions are modeled as a smooth neutralizing background. In Fig. 1, we show a sequence of four color contour plots of the laser's electric field with a common color map. The four snapshots correspond to when the laser initially impinges on the plasma and to when the head of the laser has penetrated 0.57, 0.83, and 1.82 mm into the plasma, respectively. After only 0.57 mm, i.e., $0.5x_R$, the head of the pulse has been depleted from Raman scattering while the back of the pulse has strongly self-focused. Details of this have been reported elsewhere [10]. Eventually, as seen in Fig. 1(c), the middle of the pulse is modulated from Raman forward scattering, while the back of the pulse expands and breaks up into two major filaments in which both Raman forward scattering and conventional hosing are occurring. However, later in time the pulse reaches a "final" nonlinear state, where the back of the pulse has refocused into a major filament (with two weaker filaments surrounding it) whose average position in the y

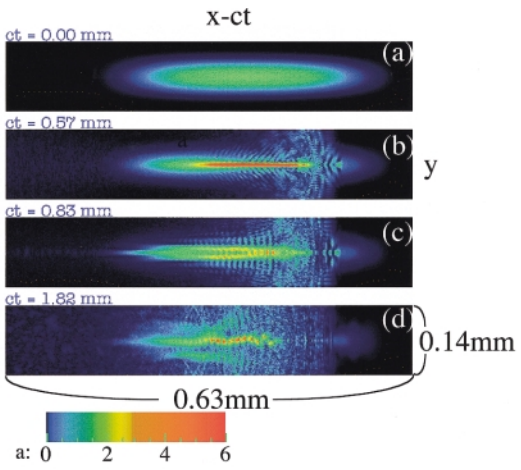

FIG. 1 (color). A sequence of color contours of the laser's electric field in units of $eE/mc\omega_0 \simeq a$. The results are from the same simulation.

 0031-9007/99/83(10)/1978(4)$15.00

direction, y_a, oscillates about the original laser axis. The intensity contours closest to the front of the pulse alternate above and below the original laser axis at a wavelength of roughly twice the plasma wavelength, $\lambda_p = 2\pi c/\omega_p$. At positions farther back, y_a is modulated at a longer wavelength—between $(5-10)\lambda_p$. This hosing behavior at wavelengths longer than λ_p, i.e., LWH, was not discussed in the earlier theoretical analyses [8,9]. We emphasize that the nonlinear evolution of the pulse is also influenced by wave breaking and intense plasma heating [12,13].

In order to present a possible explanation for LWH, we have developed a variational principle approach [14] to describe the evolution of short-pulse lasers interacting with their self-consistent wakes. The standard equations for describing short-pulse lasers, which include the lowest order relativistic corrections and assume a cold plasma, are now well established to be

$$\left(\nabla_\perp^2 - \frac{2}{c}\frac{\partial^2}{\partial\psi\partial\tau} - 2ik_0\frac{\partial}{\partial\tau}\right)a = \frac{\omega_p^2}{c^2}(1-\phi)a, \quad \text{(1a)}$$

$$\left(\frac{\partial^2}{\partial\psi^2} + \omega_p^2\right) = \omega_p^2\frac{|a|^2}{4}, \quad \text{(1b)}$$

where a is the normalized envelope for the complex vector potential of the laser, $eA/mc^2 = (a/2)\times \exp[-i\omega_0\psi]$ + c.c., ϕ is the scalar potential of the plasma, and $\psi = t - x/c$, $\tau = x/c$ are convenient variables for describing short-pulse lasers.

In the variational method a Lagrangian density $\mathcal{L}$ needs to be found for which the Euler-Lagrange equations, obtained by varying the action $S = \int dx_\perp\, d\psi\, d\tau\, \mathcal{L}$, recover Eqs. (2). We find such an $\mathcal{L}$ to be

$$\mathcal{L}(a,a^*,\phi) = \vec{\nabla}_\perp a\cdot\vec{\nabla}_\perp a^* - ik_0(a\partial_\tau a^* - a^*\partial_\tau a) - \frac{2}{c}(\partial_\psi\phi)^2 + 2\frac{\omega_p^2}{c^2}\phi^2 - \frac{\omega_p^2}{c^2}(\phi-1)|a|^2,$$

where we have dropped the so-called dispersive terms, i.e., those which give the mixed derivative term on the left-hand side of Eq. (1a) [14]. Dropping the dispersive terms leads to conservation of power, i.e., $\partial\tau\int dx_\perp |a|^2 = 0$. Anderson and Bonnedal [15] used the variational approach to study only self-focusing, which precludes any coupling to the plasma-wave wake and hence their $\mathcal{L}$ depends upon a and a^* only.

In the variational method, the complexity of the system is reduced by substituting trial functions for a and ϕ into the action and performing the $dx_\perp$ integration. To consider hosing, we assume a trial function for a of the form $a = \mathcal{A}e^{i\chi}e^{ik_y(y-y_a)}e^{-2[(y-y_a)^2+z^2]/w^2}$ and for ϕ of the form $\phi = \Phi e^{-2[(y-y_\phi)^2+z^2]/w^2}$, where the parameters $\mathcal{A}$, Φ, χ, k_y, y_a, and y_ϕ are treated as functions of (ψ,τ). The spot size w is taken to be a constant which we allow to be the same for both a and ϕ. The "centroid" variables y_a and y_ϕ measure the distance that the center of the laser and its wake are displaced from the original axis. Performing the $dx_\perp$ integration yields a reduced action which is a functional of the variational parameters, i.e., $\overline{S}(\mathcal{A},\chi,\Phi,\alpha,k_y,y_a,y_\phi) = \int d\psi\, d\tau\, \overline{\mathcal{L}}$. Varying $\overline{S}$ with respect to χ yields the power conservation law, $\partial_\tau P = \partial_\tau(\mathcal{A}^2w^2) = 0$. Variations with respect to the functions α and k_y give the relationships $\alpha = -(k_0/4)\partial_\tau(w^2)$ and $k_y = -k_0\partial_\tau y_a$, which can be substituted back into $\overline{\mathcal{L}}$ to yield the following reduced form of $\overline{\mathcal{L}}$, $\overline{\mathcal{L}}(\Phi,y_a,y_\phi)$:

$$\overline{\mathcal{L}}(\Phi,y_a,y_\phi) = -\frac{k_0^2}{4}P(\partial_\tau y_a)^2 + \frac{k_p^2}{2}\left(w^2\Phi^2 - \frac{P\Phi}{2}e^{-[(y_a-y_\phi)^2/w^2]}\right) - \frac{1}{c^2}\left[\frac{w^2}{2}(\partial_\psi\Phi)^2 + \Phi^2(\partial_\psi y_\phi)^2\right].$$

Next, we linearize the Euler-Lagrange equations of $\overline{\mathcal{L}}$ about a solution in which $y_{a0} = y_{\phi 0} = 0$ and $\Phi_0 = a_0^2/4$, giving the coupled equations for y_a and y_ϕ:

$$\partial_\tau^2 y_a + c^2 g\frac{P}{P_c}\frac{1}{x_R^2}y_a = c^2 g\frac{P}{P_c}\frac{1}{x_R^2}y_\phi, \quad \text{(2a)}$$

$$\partial_\psi^2 y_\phi + \omega_p^2 y_\phi = \omega_p^2 y_a, \quad \text{(2b)}$$

where $P/P_c = \mathcal{A}^2(k_p w)^2/32$, g is a geometric factor which is 1 in cylindrical and $2^{-3/2}$ in slab geometry (used in the simulations), and $x_R = k_0 w^2/2$ is the Rayleigh length for the equilibrium laser profile. Note that these equations are identical in form to those which describe hosing of electron beams in the ion focused regime [16], and they reproduce Eq. (5) in Ref. [8].

To discuss the growth rate and range of unstable wavelengths for hosing, we obtain a dispersion relation in the lab frame by using the transformations $\partial_\tau \to \partial_t + \partial_x$ and $\partial_\psi \to \partial_t$ and substituting solutions of the form $\exp[i(kx - \omega t)]$ into Eqs. (2), yielding $\tilde{\omega}^2(\tilde{\omega}-\tilde{k})^2 - (\tilde{\omega}^2 g(P/P_c)/\tilde{x}_R^2) - (\tilde{\omega}-\tilde{k})^2 = 0$, where $\tilde{\omega} \equiv \omega/\omega_p$, $\tilde{k} \equiv k/k_p$, and $\tilde{x}_R \equiv k_p x_R$. In Fig. 2 we plot the growth rate, i.e., the imaginary part of $\tilde{\omega}$, vs real $\tilde{k}$ for $P/P_c = 1$, i.e., a matched beam. This confirms that the peak growth rate occurs for $\tilde{k} \sim 1$, i.e., $k \sim k_p$. This region of unstable growth is related to RFS, since a plasma wave is being excited, and it is the regime discussed in Refs. [8] and [9]. However, Fig. 2 also makes clear that the range

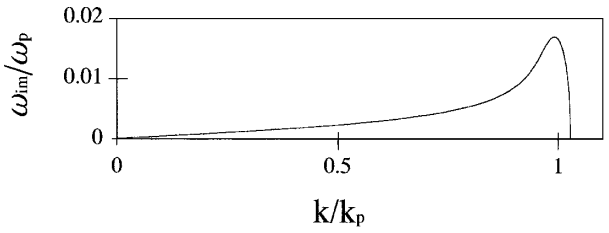

FIG. 2. The growth rate for hosing vs wave number for $\tilde{x}_R = 256$.

of unstable wave numbers extends continuously down to $\tilde{k} = 0$. This long-wavelength regime has heretofore never been discussed. This regime could have been obtained immediately if $y_\phi = y_a$ was assumed in the trial functions, which forces the centroids for ϕ and a to be in phase. In this limit, the plasma response ϕ is due almost entirely to relativistic mass corrections, i.e., no plasma waves are excited. Therefore, this long-wavelength regime is the whole beam analog to relativistic self-phase modulation (RSPM) [17]. Long-wavelength hosing is therefore physically distinct from conventional hosing in the same way that RSPM is distinct from RFS.

The spatiotemporal growth for the conventional and LWH regimes also differs. In the RFS regime, for $\tilde{\omega}$ near k_p the asymptotic spatiotemporal growth for hosing is given by [8,9] y_a or $y_\phi \sim \exp[(3^{3/2}/4) \times [g(P/P_c)\omega_p\psi]^{1/3}(\tau/\tau_R)^{2/3}]$. In the LWH regime, where the inequality $\partial_\psi^2 \ll \omega_p^2$ holds, Eq. (2b) leads to $y_\phi \cong y_a/(1 - k^2)$. Substituting this relationship into Eq. (2a) gives the spatiotemporal growth y_a or $y_\phi \sim \exp[(gP/P_c)^{1/2}(k/k_p)^{1/2}(\tau/\tau_R)]$. These expressions are only valid under the ideal conditions of cold plasmas, weakly relativistic pumps, and matched beams.

However, for current experimental parameters [18] the conditions are far from ideal. Therefore, to accurately determine the relative importance of the various regimes for hosing with respect to other self-modulational processes, we next present additional results from fully nonlinear PIC simulations. In Fig. 3 we show color contour plots of the laser's electric field in units of $eE/(mc\omega_0) \approx a$ to illustrate the final nonlinear state of short-pulse lasers from four different simulations. In each case, a 600 fs laser pulse is focused to the edge of a uniform, preformed plasma slab and the ions are a fixed neutralizing background. It is clear that for each simulation the final state shows strong self-focusing and a dominant LWH component. In Fig. 3(a), the laser's electric field is shown after a propagation distance of 1.8 mm $= 6x_R$ from a simulation with parameters identical to those in Fig. 1, except $w_0 = 10$ μm instead of 20 μm. The dominant hosing wavelength is similar to that in Fig. 1(d) but the amplitude of the centroid seems larger and the instability seems to have saturated. The spatiotemporal theory predicts that the number of e-foldings for LWH scales as $1/w_0$ for otherwise fixed parameters. This scaling is consistent with the observation from Figs. 3(a) and 1(d) that LWH is stronger when $w_0 = 10$ μm compared to when $w_0 = 20$ μm. For the parameters of this simulation, $P/P_c \simeq 6.75$ and $k/k_0 \simeq 10$, the spatiotemporal theory predicts $\sim$9 e-foldings of LWH growth, using the focused value of the spot size ($w = 5.6$ μm) and the fact that $a^2 w$ is conserved in slab geometry.

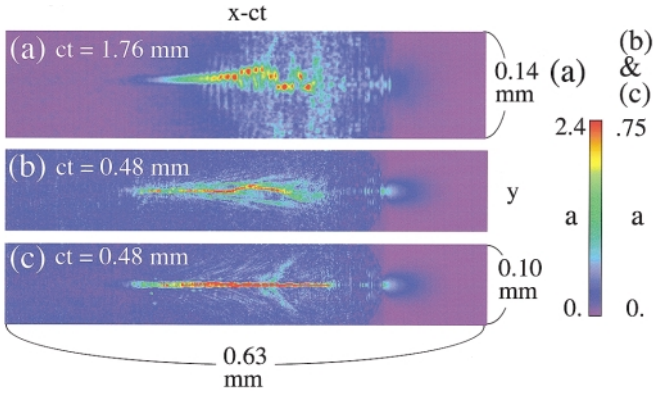

FIG. 3 (color). Color contours of the laser's electric field in units of $eE/mc\omega_0 \simeq a$ to show further evidence for long-wavelength hosing. The results are from three different simulations.

The importance of LWH is further illustrated in Fig. 3(b), which shows results from a simulation which followed 10^8 particles on a 16384 $\times$ 1024 grid. The plasma density was increased to 10^{20} cm^{-3}, i.e., $\omega_0/\omega_p = 3.3$, the laser intensity was lowered to 1.25×10^{18} W/cm^2, i.e., $a_0 = 1$, and the spot size was decreased to 6 μm, i.e., $k_p w_0 = 11.3$. Once again, after only a few (480 μm $\simeq 4x_R$) Rayleigh lengths of propagation, the laser has strongly self-focused and a LWH mode is dominant. The dominant wavelength is $\sim(15-30)k_p$ in this case. Using the self-focused spot size, the spatiotemporal theory predicts $\sim$5–8 e-foldings of LWH.

In each simulation, there is little or no evidence of the conventional (RFS) type of hosing, except for its presence in the filaments of Fig. 1(c). However, the spatiotemporal theory predicts many e-foldings of growth. Furthermore, we have independently excited both conventional and long-wavelength hosing in smaller test case simulations by adding large fictitious hosing noise sources. Therefore, the lack of RFS hosing is due to nonlinear effects. There are several possible nonlinear explanations. Because of its lower initial noise source, hosing generally occurs after the beam has strongly self-modulated from RFS and self-focusing. The occurrence of RFS divides the beam into beamlets spaced at λ_p [this is seen in Figs. 1(b) and 1(c)]. When hosing occurs, as seen in Fig. 1(d), it appears to first displace one beamlet upward and the next beamlet downward. This results in a hosing wavelength of $2\lambda_p$ and, as the laser continues to evolve, even longer wavelength modes dominate. Therefore, it appears that hosing behaves differently when other instabilities such as RFS have already grown to saturated levels. Another explanation for the lack of RFS hosing is that the plasma has been strongly heated by the time hosing occurs. RFS hosing involves the excitation of a plasma wave, which can be strongly damped at high temperatures, thereby causing a suppression of RFS hosing.

With regard to the fast ignitor, where longer pulses and higher densities are important (particularly for higher densities), the frequency of the hosing, $\omega = ck$, can be lower or on the same order as the ion plasma period, $\omega_{pi} = 4\pi e^2 n_0/m_i$. In this case, the ion dynamics cannot

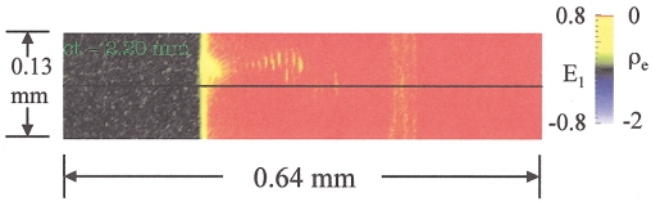

FIG. 4 (color). Color contour of electron density showing self-trapped electrons exiting the plasma. The results are from the same simulation as Fig. 3(a).

be ignored. In Fig. 3(c), we show results from an identical simulation to that shown in Fig. 3(b), except mobile hydrogenlike ions were used. The difference between the two cases is dramatic. The ion motion appears to stabilize the hosing (at least for the duration of the simulation). On the other hand, we note that in a simulation with 10 times higher intensity, i.e., $a_0 = 3$, ion dynamics did not stabilize hosing. Instead, it appeared to cause the beam to self-focus and filament differently with LWH still occurring in the individual filaments. The wavelength for hosing was shorter than $2\pi c/\omega_{pi}$ in this case. So it appears that ion dynamics can stabilize hosing when $\lambda_{\text{hosing}} \gtrsim 2\pi c/\omega_{pi}$. We also note that LWH can occur for densities above quarter critical where RFS cannot, because no plasma wave is excited. Preliminary evidence of a LWH effect has already been observed in simulations for this density regime [19]. Therefore LWH could be important for the fast ignitor fusion concept.

In conclusion, we note that LWH might have important consequences for the electron spectra generated in self-trapped acceleration experiments [18]. This is illustrated in Fig. 4, where a color contour plot of the plasma density is shown as the self-trapped electrons exit into a vacuum region. The results are from the simulation corresponding to Fig. 3(a). The black line is drawn in the middle for reference. The electrons are clearly exiting the plasma off axis by a distance ~ 10 μm, and their pattern corresponds to the laser profile in Fig. 3(a). When the plasma slab was shortened to 1 mm, no hosing was seen to occur, and the accelerated electrons were not displaced [11].

We acknowledge useful discussions with Professor T. Katsouleas, Professor C. Joshi, Professor A. Pukhov, and Professor J. C. Adam. This work was supported by DOE Contracts No. DE-FG03-92ER40727 and No. DE-FG03-98DP00211, NSF Grant No. DMS-9722121, and LLNL Contract No. W-7405-ENG-48.

[1] T. Tajima and J. M. Dawson, Phys. Rev. Lett. **43**, 267 (1979); E. Esarey *et al.*, IEEE Trans. Plasma Sci. **24**, 252 (1996), and references therein.
[2] Special issue, edited by W. B. Mori [IEEE Trans. Plasma Sci. **PS-21(1)**, (1993)].
[3] M. Tabek *et al.*, Phys. Plasmas **1**, 1626 (1994).
[4] P. Sprangle *et al.*, IEEE Trans. Plasma Sci. **PS-15**, 145 (1987).
[5] W. B. Mori *et al.*, Phys. Rev. Lett. **72**, 1482 (1994); W. B. Mori, IEEE J. Quantum Electron. **33**, 1942 (1997).
[6] T. M. Antonsen, Jr. and P. Mora, Phys. Rev. Lett. **69**, 2204 (1992); N. E. Andreev *et al.*, Sov. Phys. JETP Lett. **55**, 571 (1992).
[7] E. Esarey *et al.*, Phys. Rev. Lett. **72**, 2887 (1994).
[8] P. Sprangle *et al.*, Phys. Rev. Lett. **73**, 3544 (1994).
[9] G. Shvets and J. S. Wurtele, Phys. Rev. Lett. **73**, 3540 (1994).
[10] K-C. Tzeng *et al.*, Phys. Rev. Lett. **76**, 332 (1996); K-C. Tzeng, Ph.D. dissertation, UCLA, 1998.
[11] K-C. Tzeng *et al.*, Phys. Rev. Lett. **79**, 5258 (1997).
[12] K-C. Tzeng and W. B. Mori, Phys. Rev. Lett. **81**, 104 (1998).
[13] A. Pukhov and J. Meyer-ter-Vehn, Phys. Plasmas **5**, 1880 (1998).
[14] B. J. Duda and W. B. Mori, Bull. Am. Phys. Soc. **43**, 1658 (1998); (to be published).
[15] D. Anderson and M. Bonnedal, Phys. Fluids **22**, 105 (1979).
[16] D. H. Whittum *et al.*, Phys. Rev. Lett. **67**, 991 (1991).
[17] C. E. Max *et al.*, Phys. Rev. Lett. **33**, 209 (1974); C. J. McKinstrie and R. Bingham, Phys. Fluids B **4**, 2626 (1992).
[18] A. Modena *et al.*, Nature (London) **337**, 606 (1995); D. Gordon *et al.*, Phys. Rev. Lett. **80**, 2133 (1988); D. Umstadter *et al.*, Science **273**, 472 (1996); R. Wagner *et al.*, Phys. Rev. Lett. **78**, 3125 (1997); C. A. Coverdale *et al.*, Phys. Rev. Lett. **74**, 4428 (1995); A. Ting *et al.*, Phys. Plasmas **4**, 1889 (1997).
[19] J. C. Adam (private communication).